Colloid Micro-Thruster (CMT) Component Development & Testing Towards Meeting LISA Mission Requirements

IEPC-2019-255

Presented at the 36th International Electric Propulsion Conference
University of Vienna • Vienna, Austria
September 15-20, 2019

N. Demmons[1], N. Alvarez[2], Z. Wood[3], M. Strain[4]
Busek Company, Natick, MA, 01760, USA

and

J. Ziemer[5]
Jet Propulsion Laboratory, California Institute of Technology, 4800 Oak Grove, Pasadena, CA, 91109, USA

Abstract: The recently completed European Space Agency Lisa Pathfinder (LPF) mission was a significant success with regards to demonstrating technologies necessary for development of a platform suitable for space-based gravitational wave detection. As part of the NASA Space Technology 7 (ST7) program, a Disturbance Reduction System (DRS) was developed and flown on LPF to demonstrate a precision attitude control system consisting of: two Colloid Micro-Thruster (CMT) Clusters developed by Busek Company in cooperation with JPL, each comprising four fully independent colloid thrusters and associated electronics, and an Integrated Avionics Unit (IAU) developed by JPL, containing drag-free control algorithms developed at NASA Goddard Space Flight Center (GSFC). During LPF flight operations the ST7-DRS system met all system-level requirements, with over 20,000 hours of cumulative operation being demonstrated across the eight colloid thrusters. This was an unprecedented success for such a rapidly developed technology and efforts have pivoted to preparation for the follow-on mission. Lessons learned from development, flight hardware production, and flight operations were compiled and prioritized with regards to their relevance for LISA. Updates have focused on adding redundancy (e.g. series/parallel valve configurations and redundant thruster heads), improved assembly yield to support larger scale production, and repackaging to meet updated spacecraft designs. New and updated feed system elements have been fabricated and assembly processes validated, providing preliminary production yield data for the future flight build. Components were subjected to vibration and thermal testing environments and proper function verified. Next steps entail component integration into major subassemblies, and continued environmental testing.

I. Nomenclature

c	=	specific heat capacity	μ	=	dynamic viscosity
K	=	coef. of thermal conductivity	Q	=	volumetric flow rate
L	=	capillary/tube length	Q	=	heat capacity
M	=	mass	Q_c	=	conductive heat transfer rate
P	=	pressure differential	r_i	=	capillary/tube inner radius

[1] Director, Micro-Propulsion Group, 11 Tech Circle, Natick MA, 01760 and AIAA Senior Member
[2] Research Engineer, Micro-Propulsion Group, 11 Tech Circle, Natick MA, 01760, Member AIAA
[3] Research Engineer, Micro-Propulsion Group, 11 Tech Circle, Natick MA, 01760, Member AIAA
[4] Research Engineer, Design Group, 11 Tech Circle, Natick MA, 01760, Member AIAA
[5] NASA LISA Micro-propulsion Tech. Dev. Lead, 4800 Oak Grove, Pasadena, CA, 91109, AIAA Senior Member

r_o	=	capillary/tube outer radius
ΔT	=	temperature difference
Z_C	=	capillary impedance
Z_{MV}	=	microvalve impedance
Z_T	=	thruster flow impedance

II.Introduction

Electrospray (or colloid) thrusters are a form of electric propulsion well suited for sub-micronewton precision thrust applications, such as the European Space Agency (ESA) Laser Interferometer Space Antenna (LISA) mission. They function by electrostatically accelerating nanometer-sized droplets and/or ions emitted from what is commonly referred to as a Taylor cone, generating up to serval micronewtons per emission site. Busek has developed multiple electrospray thruster configurations, the most mature of which was developed for the ESA LISA Pathfinder (LPF) mission. A table of key LPF colloid thruster performance metrics is shown in Table 1 that highlight the mission-specific focus on thrust precision and noise. These requirements were met and generally are the same for LISA. However, the operational life for the flagship LISA mission is 4 years. System updates are anticipated in order to meet this jump in thruster life. Additionally, required maximum thrust levels are being studied, with larger spacecraft designs indicating that increased thrust may be necessary to oppose solar pressure.

Table 1. ST7-DRS key thruster requirements.

Requirement	Value
Thrust Range (μN)	5-30
Thrust Precision (μN)	0.1
Thrust Noise (μN/√Hz)	0.1
Thrust Full Range Response (sec)	<100
Operational Life (days)	90

The European LISA Pathfinder (LPF) mission was a significant success with regards to demonstrating technologies necessary for development of a platform suitable for space-based gravitational wave detection. As part of the Space Technology 7 (ST7) program, a Disturbance Reduction System (DRS) was developed and flown on LPF to demonstrate a precision attitude control system consisting of: two Colloid Micro-Thruster (CMT) systems developed by Busek Company in cooperation with JPL, each comprising four fully independent colloid thrusters and associated electronics, and an Integrated Avionics Unit (IAU) developed by JPL, containing drag-free control algorithms developed at NASA Goddard Space Flight Center (GSFC). The development of the capillary-emitter based electrospray system used has been previously reported.[1,2,3,4,5,6] The fully-fueled flight units, shown in Figure 1, were delivered to JPL in 2008.

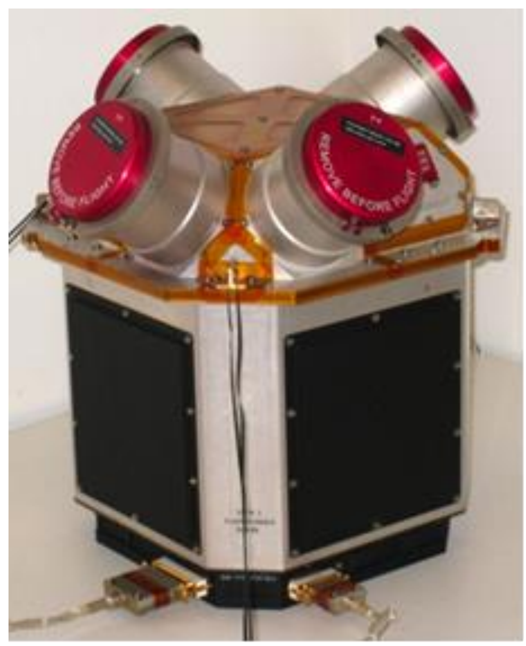

Figure 1. Colloid Micro-Thruster.

Initial on-orbit commissioning of the CMT's took place in January of 2016, with multiple science collection campaigns performed throughout 2016 and 2017. During LPF flight operations the ST7-DRS system met all system-level requirements, with over 20,000 hours of cumulative operation being demonstrated across the eight colloid thrusters.[7,8,9] This was an unprecedented success for such a rapidly developed technology and efforts have pivoted towards preparation for the LISA mission.

III. System-Level Design

System architecture changes from the flight-qualified system flown as part of the LISA Pathfinder mission and that presently being developed for LISA are largely driven by the addition of redundancy. As is apparent in in the LPF cluster feed system and thruster block diagram (Figure 2, left), there were multiple single point failure locations within the system. For example, each thrust axis had only a single thruster with no redundant heads, and each feed system contained only a single flow control valve. In contrast, the preliminary LISA system configuration (Figure 2, right) has both series redundancy via multiple valves per feed system, as well as full parallel redundancy by way of a completely independent secondary Thruster String Assembly (TSA) per thrust axis.

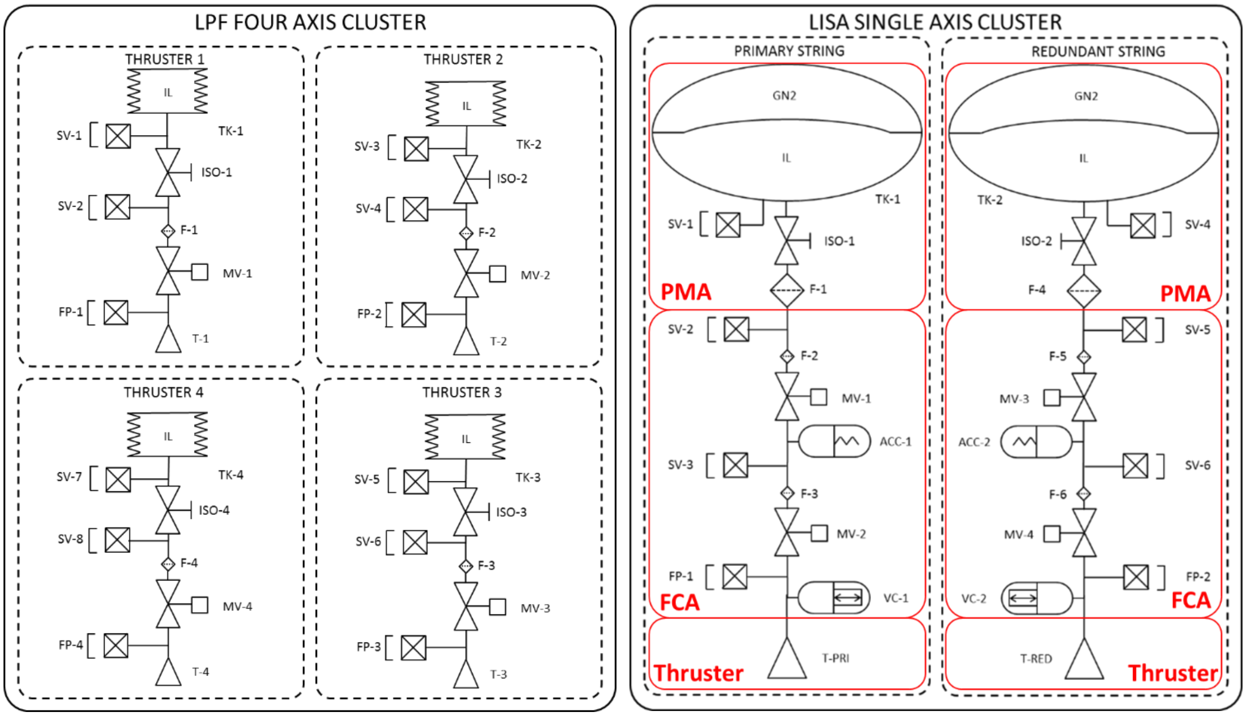

Figure 2. LISA Pathfinder (left) and preliminary LISA (right) mechanical block diagrams.

The present Colloid Micro-Thruster System (CMTS) assembly consists of a fully independent primary and redundant Thruster String Assembly (TSA). The TSA has been segregated into three primary mechanical sub-assemblies. The Propellant Management Assembly (PMA) consists of non-microfluidic propellant storage portion of the feed system from the propellant tank to the input of the Flow Control Assembly (FCA) at fill/drain Service Valves (SV-2 & SV5). The FCA (Figure 3, left) consists of the multiple active and passive flow control elements necessary to regulate µL/min flowrates to the thruster, with less than nL/sec resolution. This includes two proportional control Microvalves (MV-1 to MV-4) per string, one accumulator (ACC-1 & ACC-2) located between the two series valves, and a feed system downstream volume management device called a Volume Compensator (VC-1 & VC-2). These elements work in tandem to not only regulate precision flow, but also to mitigate both operational and non-operational thermal conditions that the system may encounter during the mission. Elements within the FCA are closely integrated in order to minimize dead volumes, which aids in propellant filling, thermal management, and thruster startup/shutdown operations. The thruster head (Figure 3, right) consists of nine capillary-based electrospray emitters provided pressurized propellant flow from a common manifold. The thruster head also includes the electrostatic grid subassembly that accelerates the electrospray plume through a two-grid configuration. Additionally, the electrostatic grids are fabricated from porous metal in order to collect and sequester any potential plume interception and prevent thruster electrical shorting through the accumulation of the conductive ionic liquid propellant.

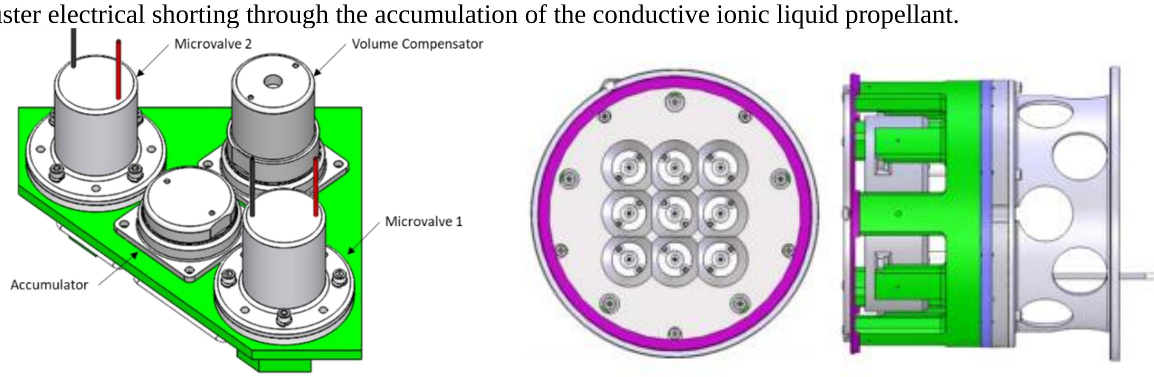

Figure 3. Flow Control Assembly (left) consisting of an Accumulator, Volume Compensator, and two Microvalves. Baseline preliminary thruster head design (right) for LISA consisting nine individual capillary emitters.

A. System-Level Configuration

Potential spacecraft configurations for the LPF follow-on mission, the Laser Interferometer Space Antenna (LISA), were initially developed as part of a study by the European Space Agency (ESA) Concurrent Design Facility (CDF). Busek's preliminary system-level designs were responsive to the results of that study and have been previously reported.[10] Presently, multiple aerospace prime contractors are maturing the spacecraft and mission design as part of a Phase A study, including examining engineering trades between cold gas micro-thruster and CMT alternatives.

Based on updated component level design and relevant LISA spacecraft designs, CMTS mass, volume, and power budgets have been estimated and compared to alternative cold gas propulsion options, with a preliminary design shown in Figure 4. Due to system complexity, colloid thrusters for LISA are anticipated to have larger system dry masses, as compared to cold gas. However, due the extended duration of the mission and higher specific impulse of colloid thrusters, total mass savings are considerable and result in an estimated 50% reduction in propulsion system wet mass, corresponding to several hundred kilograms of mass savings across the constellation of three spacecraft. Volumetric savings are similarly significant due to higher specific impulse and higher propellant storage density (1.53g/cc). Through novel designs and additional light-weighting efforts, Busek has further reduced system dry mass and models used to support spacecraft design trades have been updated.

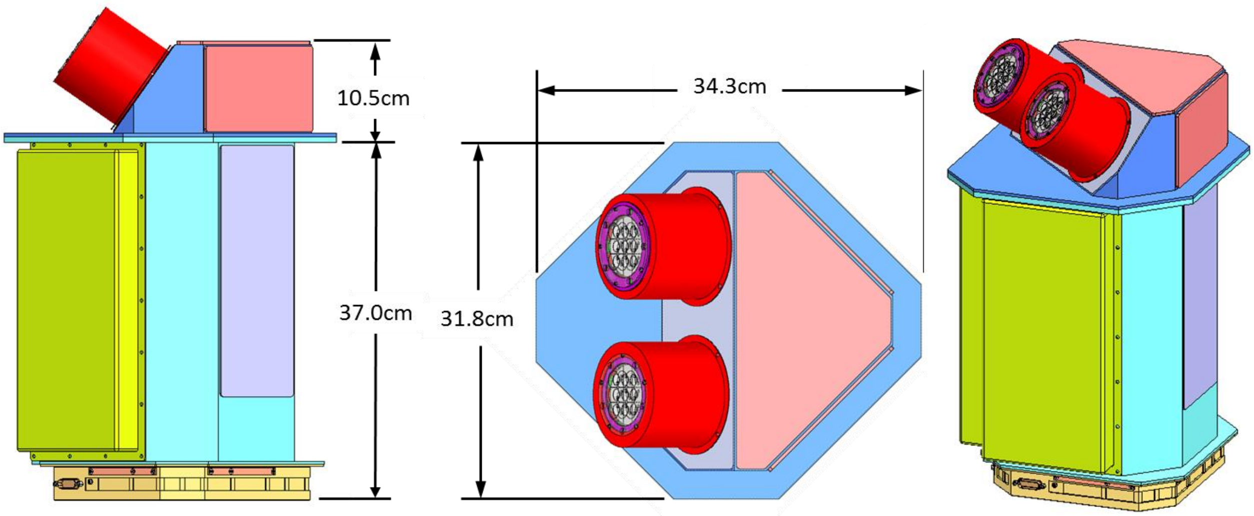

Figure 4. Updated CMTS design for a single thrust axis per cluster configuration. Image taken from ref (10).

B. CMTS Thrust Range

ESTEC Concurrent Design Facility mission study results indicated that the size of the LISA spacecrafts will likely be considerably larger than that flown as part of the LISA Pathfinder mission. Overall spacecraft size is a key driver of system design, as the primary function of the science mode propulsion system is to oppose the pressure applied on the spacecraft by the solar winds. As an initial point of comparison for predicted solar pressure, the LISA Pathfinder spacecraft had a 2.1m diameter solar panel, which, resulted in 24.9μN of solar pressure based on calculated thrust levels and known thruster pointing angles (Table 2 & Figure 5). Alternatively, the preliminary LISA spacecraft designs are rectangular, with solar panel dimensions of 3m x 4.75m. This constitutes a greater than 4X increase in solar panel area and proportional increase in solar pressure.

Table 2. Estimated solar pressure on the LPF spacecraft based on calculated thrust and known thrust vectors.

Solar Pressure, LPF Flight Data (2.1m dia.)				
Thruster	Thrust (μN)	X Angle (deg)	Y Angle (deg)	Z Thrust (μN)
1	10.1	65	35	-3.5
2	10.1	65	35	-3.5
3	16.8	45	35	9.7
4	16.8	45	35	9.7
5	10.1	65	35	-3.5
6	10.1	65	35	-3.5
7	16.8	45	35	9.7
8	16.8	45	35	9.7
Solar Pressure Estimate (μN):				24.9
Solar Pressure/Area (μN/m^2):				7.2

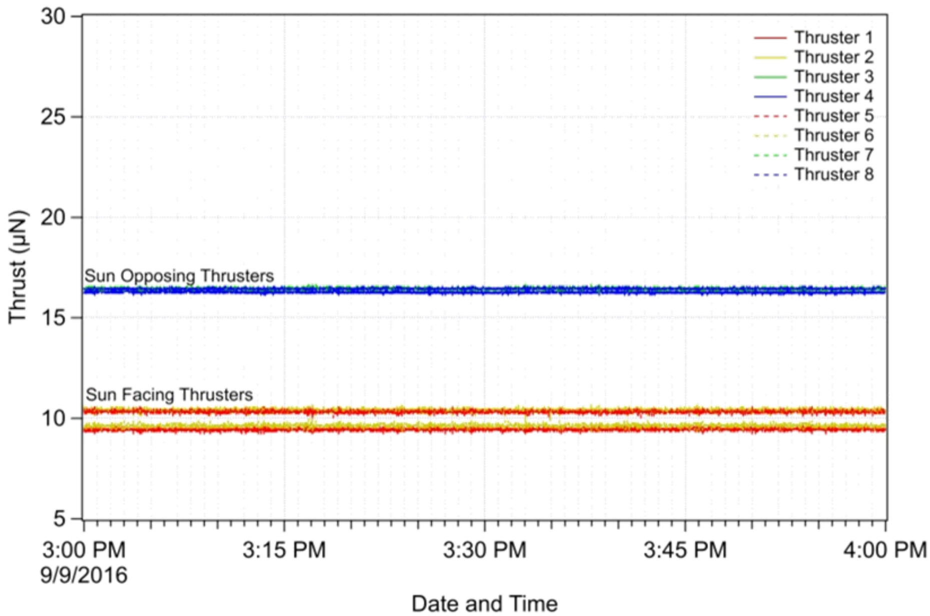

Figure 5. Calculated thrust levels for all eight LPF colloid thrusters from in-space telemetry.

Table 3. Colloid Micro-Thruster System mass estimate with ~35µN maximum thrust, after component light-weighting.

Mass Type	Component	Qty	Mass (kg)	Total (kg)
Fixed Masses	Microvalve 1	2	0.132	0.264
	Accumlator	2	0.054	0.108
	Microvalve 2	2	0.132	0.264
	Volume Compensator	2	0.112	0.224
	Feed System Manifold	2	0.218	0.436
	PPU	2	0.942	1.884
	DCIU*	1	0.746	0.746
Variable Mass	Propellant (6yrs @ 20µN)	2	1.531	3.061
	Tank	2	0.614	1.228
	Thruster	2	0.498	0.996
	TSA Structure	2	0.229	0.458
	CMTS Structure	1	1.934	1.934
9 Emitter Primary/Redundant CMTS			Dry Mass:	6.609
			Margin:	20%
			Dry Mass(w/Margin):	7.931
			Wet Mass:	9.670
			Margin:	20%
			Wet Mass(w/Margin):	11.604

*Mass assumes one DCIU per primary/redundant string, future mass savings likely

In response to the increasing size of the LISA spacecraft and to aid in ESA design trades, Busek has developed system configuration tools that predict CMTS mass, volume, and power, based on required nominal and maximum thrust. While the mass of some system elements scale with respect to thrust (e.g. thruster, tank, & propellant loading), others do not and require little to no changes to meet increased thrust requirements (e.g. flow control elements & electronics). Recently, component designs were reviewed as part of a light-weighting exercise to reduce system dry mass. As prior efforts had focused on functionality retention and not mass reduction, considerable savings were identified at the part-level. The mass of a single primary-redundant CMTS, including all system elements shown in Figure 2, was estimated and is compiled in Table 3. No significant mass reductions were assumed for the microvalves, as the design is a critical system element that is mature and on its 4th generation design revision. Mass reductions for new system elements (Accumulator & Volume Compensator) were relatively modest, as they represent a small fraction of the overall mass of the system. Thruster mass reductions were focused on structural improvements away from the emitter and grid assembly, thus avoiding changes that could impact performance. Electronics housing mass savings were assumed, as these electronics are likely to be more integrated into the overall spacecraft, requiring less structural support than was needed for the LPF design. Propellant loading is a major system mass driver and is related to mission life. The present methodology for meeting the planned 4-year primary and 6-year extended mission is to carry sufficient propellant in both the primary and redundant thruster strings for 6 years of operation (primary mission + 50%). In this configuration, the colloid thrusters will have sufficient consumables for 12 years of science, while not requiring use of redundant thrusters until 2 years into the extended mission.

CMTS system mass was calculated assuming the potential for a 4X increase in required thrust, as may be necessary based on preliminary LISA spacecraft designs. Fixed masses, such as the components within the FCA did not increase; however, propellant loading increased considerably, as shown in Table 4. Additional structure was assumed to fixture and house an overall larger system. Thruster mass increased, again taking little minimal mass savings in the emitter and grid assemblies, as their designs perform critical functions related to performance and life. Considerable mass savings were possible within the thruster body itself, as components that were no longer wetted by the propellant were switched to lighter materials once freed from material compatibility constraints.

Digital Control Interface Unit (DCIU) and Power Processing Unit (PPU) masses were relatively unchanged for increased thrust CMTS variants traded. However, once the present trade assumes one DCIU per primary-redundant string, which will likely not be the case. Additional mass savings are likely once the final s/c configuration is known and the DCIU can be updated to control multiple CMTS's. The existing electronics are sufficient to support increases in electrospray beam current. A transition to higher resolution analog to digital converters (ADC's) would be necessary to maintain beam current resolution, which impacts thrust precision. Use of 12bit ADC's for LISA Pathfinder resulted in a 6nA beam current resolution, which was roughly equivalent to 0.1μN very close to the required thrust precision for LISA. Flight qualified 16bit ADC's are now available and would achieve even lower beam current resolution, even with an increased current measurement range.

Table 4. Colloid Micro-Thruster System mass estimate with ~150μN maximum thrust, after component light-weighting.

Mass Type	Component	Qty	Mass (kg)	Total (kg)
Fixed Masses	Microvalve 1	2	0.132	0.264
	Accumlator	2	0.054	0.108
	Microvalve 2	2	0.132	0.264
	Volume Compensator	2	0.112	0.224
	Feed System Manifold	2	0.218	0.436
	PPU	2	0.942	1.884
	DCIU*	1	0.746	0.746
Variable Mass	Propellant (6yrs @ 80μN)	2	6.123	12.246
	Tank	2	1.512	3.024
	Thruster	2	1.532	3.064
	TSA Structure	2	0.436	0.872
	CMTS Structure	1	4.626	4.626
36 Emitter Primary/Redundant CMTS			Dry Mass:	15.513
			Margin:	20%
			Dry Mass(w/Margin):	18.616
			Wet Mass:	27.759
			Margin:	20%
			Wet Mass(w/Margin):	33.311

*Mass assumes one DCIU per primary/redundant string, future mass savings likely

CMTS mass was calculated for multiples of nine emitters in order to assess trends in system mass as the required thrust is increased, with the results shown in Figure 6. Increasing the number of emitters not only impacts maximum thrust, but also increases the minimum thrust, as operating the emitters close to their minimum flow can result in intermittent operation that would increase thrust noise beyond the <0.1μN/√Hz requirement. CMTS mass discussed in Table 3 and Table 4 are shown graphically in Figure 6. Propellant mass estimations were calculated under the assumption of steady state operation at a nominal thrust level that places the thruster in the middle of its throttling range to ensure rapid dynamic response to changing thrust requests from the host spacecraft. It is apparent that as required thrust levels increase, more favorable wet/dry mass ratios are achieved, largely driven by significantly increased propellant loadings under partially fixed dry mass conditions. Calculations for minimum and maximum thrust assume a nominal thruster temperature of 25°C; however, a slightly larger throttling range is possible adjusting the thruster temperature, thus impacting the physical properties (e.g. viscosity & electrical conductivity) of the ionic liquid propellant. As part of the LPF effort, the thruster demonstrated operation from 10°C, which would provide a higher maximum thrust, to 30°C, which could provide a lower minimum thrust. Depending on the operational design of the spacecraft, this larger throttling range on longer time scales may be favorable.

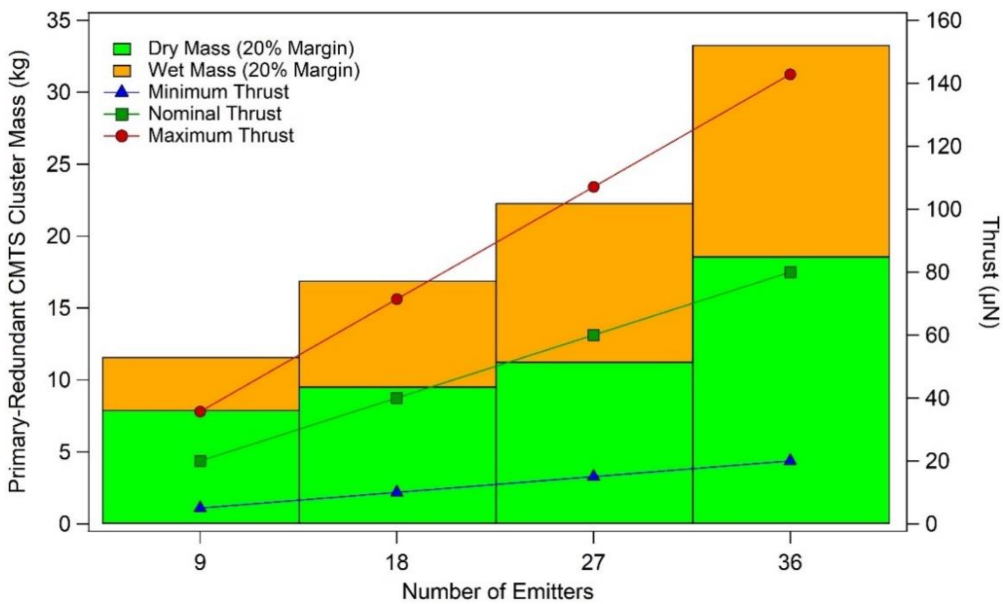

Figure 6. CMTS dry/wet mass and thrust range, with respect to scaling the number of capillary emitters.

C. Feed System Support for Increased Thrust

Given the likelihood of increased thrust requirements for the LISA mission, a feed system analysis was performed to assess the ability of the baseline feed system to support the increased flow commensurate with higher thrust. Existing validated flow models were used to assess feed system margin with respect to required flow for maximum thrust. Busek has a more mature feed system and thruster performance model that captures dynamic behavior and incorporates new system elements discussed herein (Accumulator & Volume Compensator); however, for an overall steady state flow margin assessment comparison between LPF and LISA, a basic resistive network, as in shown ***Figure 7***, will suffice. The nature of the microvalve impedance is more complicated than a simple proportionally controlled impedance. When modeled dynamically the model includes all critical functions of the microvalve, but will not be discussed in detail here. In the resistive network shown, the hydraulic impedance and flow rate *Z* and *Q*, are equivalent to resistance and flow rate *R* and *V*, respectively.

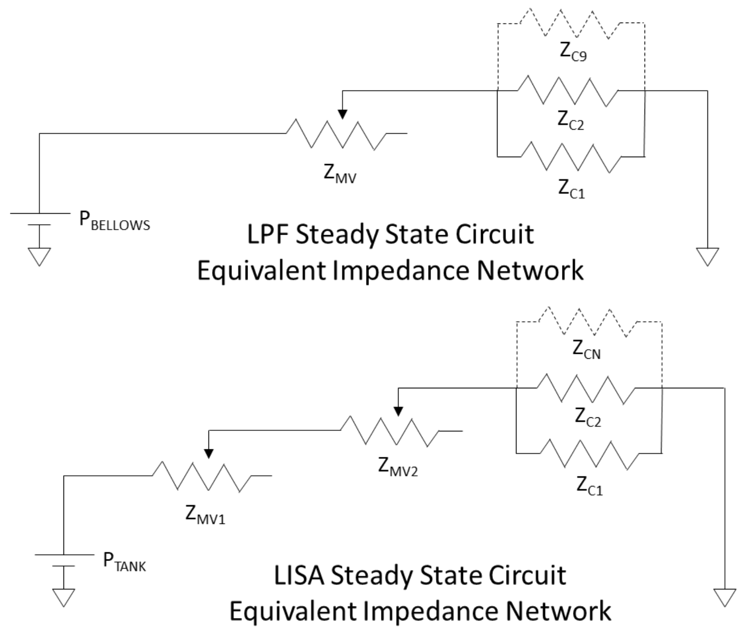

Figure 7. Resistive flow impedance network for both LPF (left) and proposed LISA (right) feed system designs.

The hydrodynamic resistance of a capillary tube, Z_C, can be calculated via Eq. (1):

$$Z_C = \frac{8\mu L}{\pi r^4} \tag{1}$$

where μ is the kinematic viscosity of the fluid, *L* the length of the tube, and *r* is the tube diameter. However, the thrust generated from a singular capillary emitter is not useful and Busek fabricates arrays of impedance matched emitters that draw propellant from a common manifold. In such a case Eq. (2) can be used to calculate the overall flow impedance of the emitter array, Z_T, via equations for parallel impedance.

$$Z_T = \frac{1}{\frac{1}{Z_{C1}}+\frac{1}{Z_{C2}}\ldots+\frac{1}{ZCn}} \tag{2}$$

Finally, steady state flow, *Q*, through each of the feed systems shown in Figure 7 is calculated using Eq (3), where ΔP is the total pressure drop across the feed system.

$$\mathrm{Q} = \frac{\Delta P}{Z_{MV1}+Z_{MV2}+Z_T} \tag{3}$$

For the LISA Pathfinder system, Busek used a spring-pressurized metal bellows that provided a continuous 1atm of pressure to a feed system consisting of a singular microvalve. The required min/max flows, as well as the corresponding beam currents are shown in Figure 8, overlaid with model predictions for the LPF colloid feed system. Results suggest that the prior flight-qualified system had a flow capability 3.6 times greater than that required to reach maximum thrust. This generally limited the operational voltage on the piezo element within the valve to a range of

10V to 15V. The general shape of the flow curve is dominated by the hysteresis of the piezo actuator during initial opening as well as transition to valve orifice limited flow at full open.

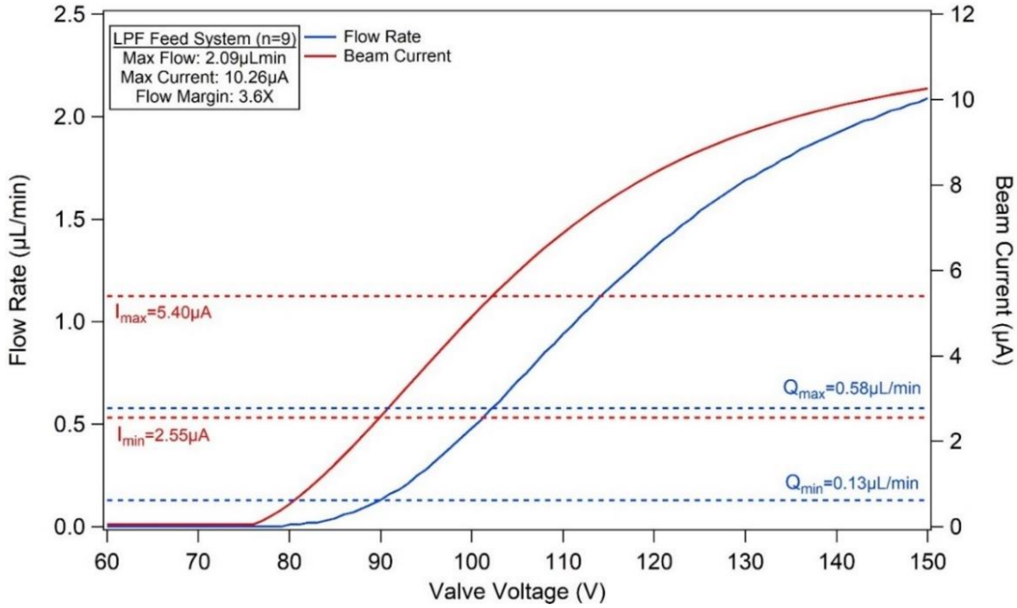

Figure 8. Model of colloid feed system flown on LPF, overlaid with minimum & maximum operating conditions.

The feed system for the LISA CMTS differs from the LPF system in that it has eliminated the spring-loaded bellows in favor of a diaphragm tank to reduce mass. Propellant is supplied via a gas-pressurization operating in a "blow-down" configuration. Under previous efforts, a prototype tank was designed and successfully tested at beginning-of-life (BOL: 4atm) and end-of-life (EOL: 2.5atm) conditions. The feed system model was updated to account for the flow impedance of two valves, as well as new calculated thruster impedances commensurate with 36 capillary emitters operating in parallel. Feed system flow margin with respect to maximum thrust conditions was again estimated at BOL and EOL, with EOL being considered worst-case conditions. As can be seen in Figure 9, similar flow margins are achieved at EOL (2.7X), as compared to that used for LPF (3.6X). The increase in the flow necessary for a 36 capillary emitter thruster are offset by the increase propellant supply pressure, resulting in similar margins. No feed system modifications are required in order to support potential increased thrust requirements as envisioned by the ESTEC CDF study.

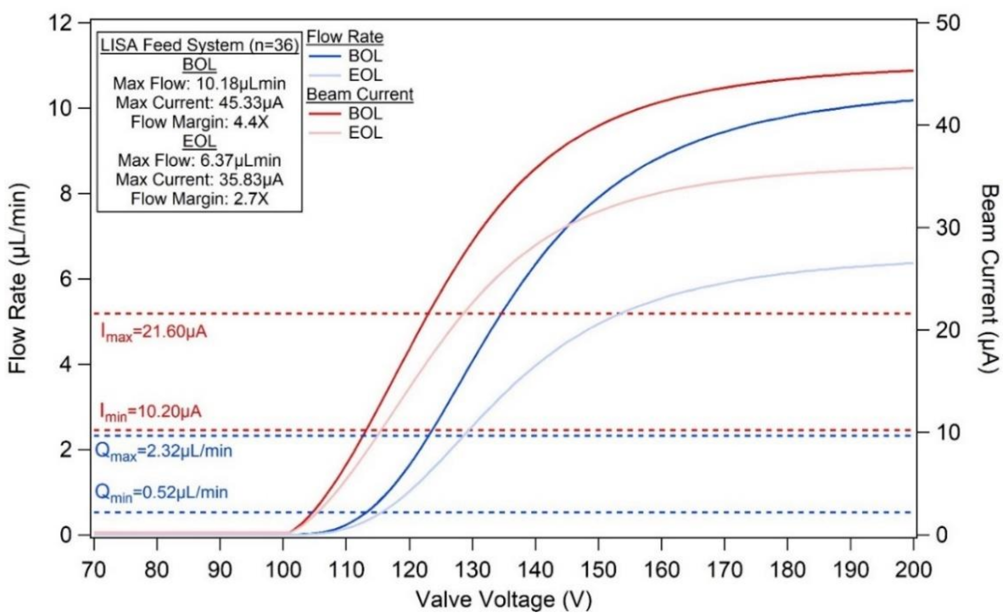

Figure 9. CMTS feed system flow capability at BOL & EOL, compared to required flow for a 36-emitter thruster head.

IV.Component-Level Fabrication & Testing

A. Microvalve

The in-house developed microvalve (Figure 10) has been matured through multiple design revisions over the course of nearly 20 years. Initial 1st generation valves were used for early tests prior to the LPF mission, with the 2nd generation being used for flight. However, while meeting the flow precision and environmental requirements, the complexity of these early designs resulted in relatively low production yields that would not be suitable for the number of valves that would be needed for the LISA constellation. Through funding from the NASA Strategic Astrophysics Technology (SAT) program, a 3rd generation valve was developed that miniaturized the valve, while significantly reduced part count and increasing production yield to 80%. More recently, and as part of incorporation of LPF lessons learned, a 4th generation microvalve has been designed, fabricated, and it now undergoing testing. Advancements in this generation include improving production yield of key subassemblies within the valve, as well as incorporating high voltage isolation back into the design that was not present as part of the 3rd generation design. Valve fabrication and assembly fixtures were also upgraded to accommodate the batch production that will be necessary to support future production needs.

Figure 10. 4th generation microvalve.

1. Vibrational Testing

Functional testing of microvalves prior to integration into ionic liquid feed system were performed using dry nitrogen. Prior to vibration testing a nitrogen flow curve was obtained for comparison to post-vibe valve performance (Figure 15, left). Testing to system-level acceptance or qualification levels could have resulted in an over testing of the valve at the component-level and vibration requirements are not yet available for the LISA mission; therefore, vibration testing was performed per NASA General Environmental Verification Standards (GEVS) for component-level workmanship (Table 5). Per typical procedures the microvalve was vibration tested in all three axes, with low-level sine sweeps performed before and after a 60 second random vibe to assess for changes in response that could potentially indicate damage. A control accelerometer mounted to the vibration test fixture was used for closed loop control of the vibration table to the desired levels, while a second accelerometer mounted to the top of the microvalve body was used for measuring the response of the device under test.

Table 5. GEVS component minimum workmanship random vibration test levels for 45.4kg (100lbs) or less.

Frequency (Hz)	ASD Level (g^2/Hz)
20	0.01
20-80	+3 dB/oct
80-500	0.04
500-2000	-3 dB/oct
2000	0.01
Overall	6.8 g_{rms}

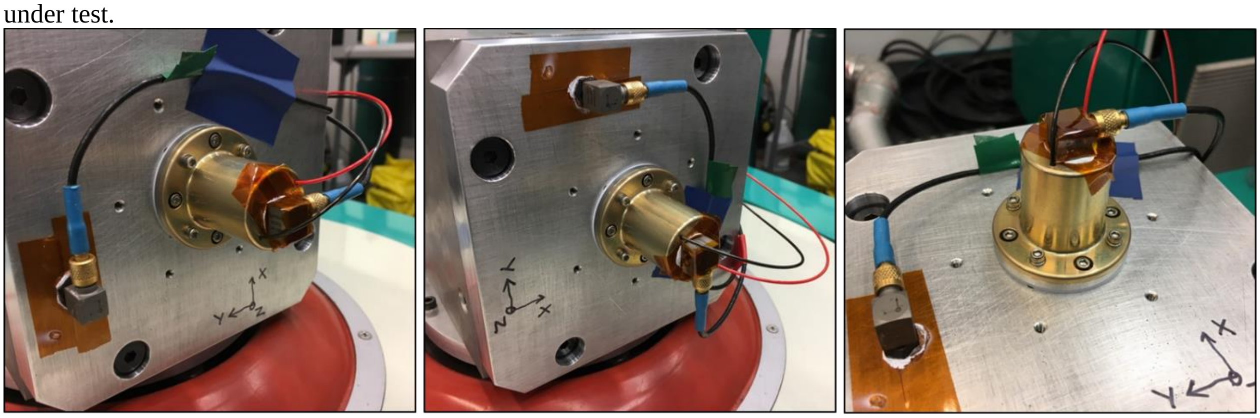

Figure 11. 4th generation piezo-actuated microvalve undergoing vibration testing to GEVs workmanship levels.

The response of the microvalve-mounted accelerometer is shown below for Z-axis low-level pre-vibe sine sweep (Figure 12), random vibe (Figure 13), and post-vibe low-level sine sweep (Figure 14). Vibration levels, at the vibe fixture interface, as measured by the fixture mounted accelerometer were within specifications for the GEVS workmanship vibe. From both the sine sweeps and random vibe response curves, there is an apparent response at approximately 180Hz. It should be noted that the increase in response at approximately 180Hz is a artifact of the test setup and is a result of mass imbalances that place the center of gravity of the test fixture off slightly off of the vibe axis, and is present in absence of the device under test.

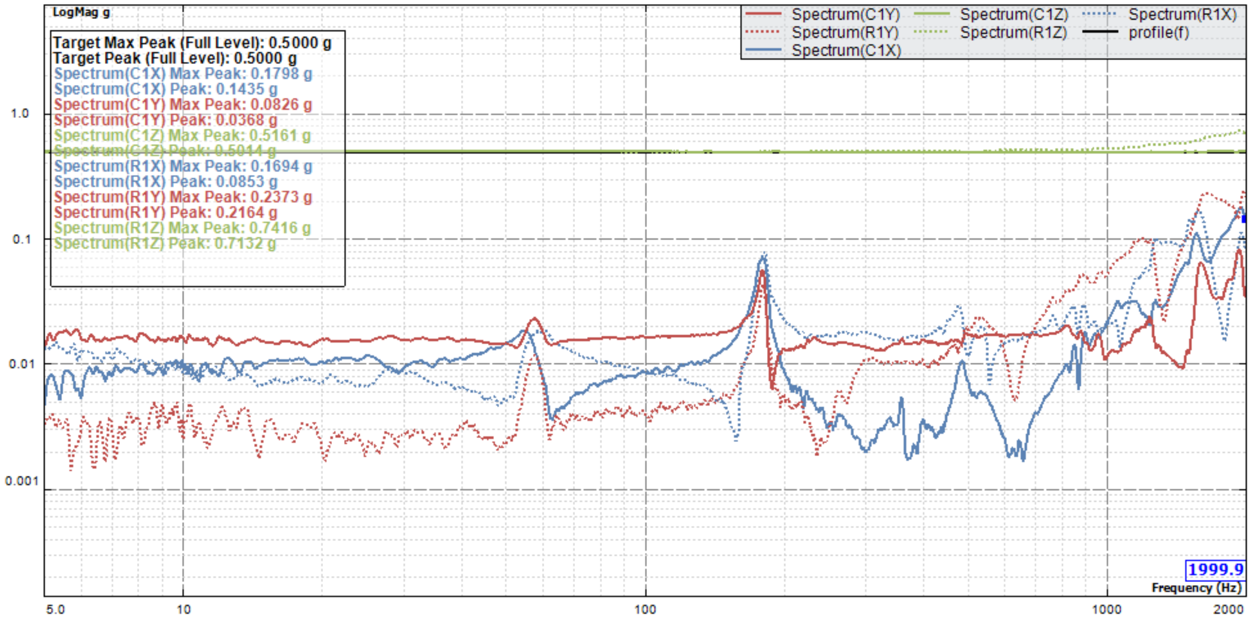

Figure 12. Pre-random vibe low-level sine sweep.

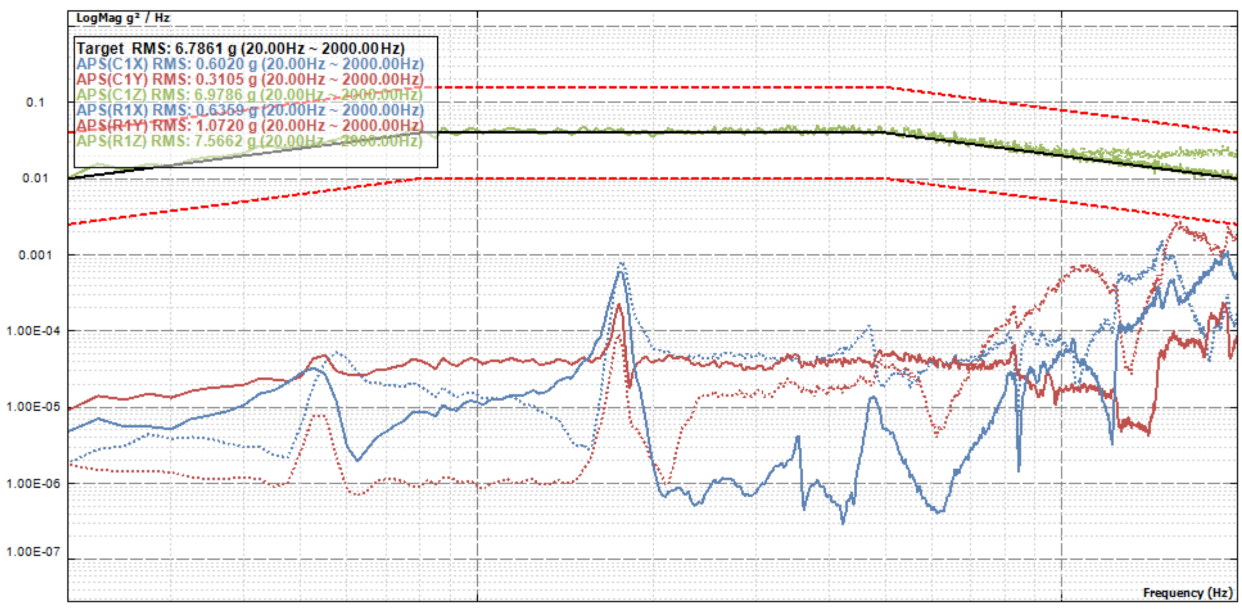

Figure 13. Microvalve z-axis random vibration.

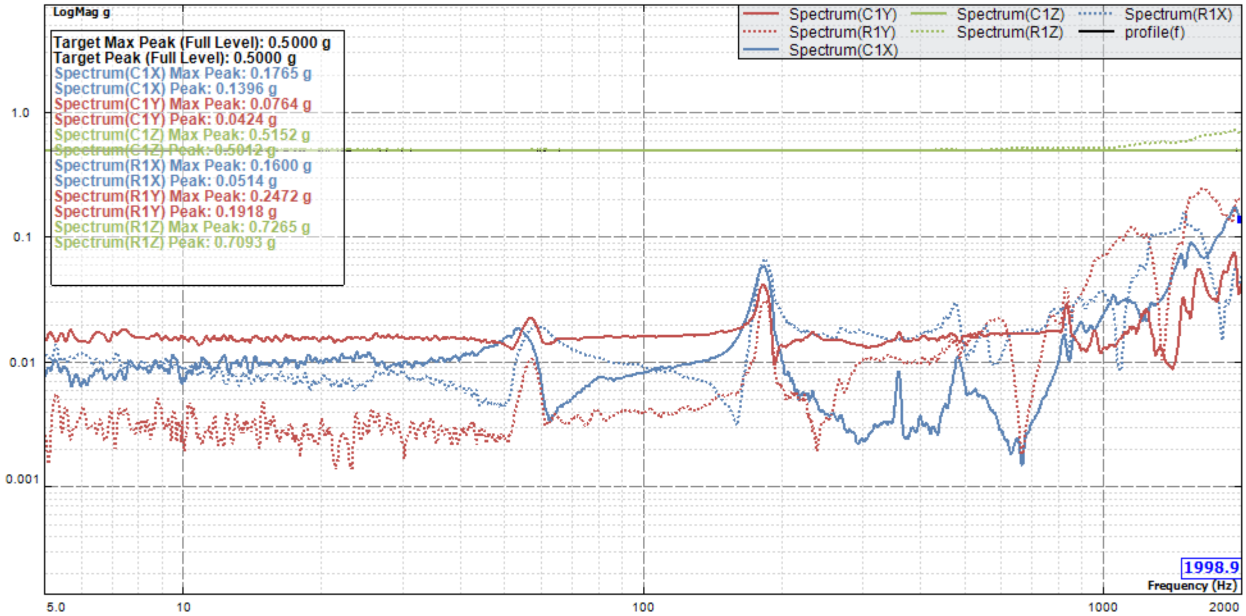

Figure 14. Post-random vibe low-level sine sweep.

After completion of vibration testing, an additional nitrogen flow curve was obtained and compared against pre-vibe results (Figure 15, right). Both pre and post vibration testing flow curves were assessed for opening and closing voltage, hysteresis, and maximum flow. Flow curve opening and closing data were fit with a Hill equation described by Eq (5):

$$Q = Q_{min} + \frac{Q_{max} - Q_{min}}{1 + \left[\frac{V_{1/2}}{V}\right]^{rate}} \tag{5}$$

where Q is the volumetric flowrate, Q_{min} the minimum flow rate, Q_{max} the maximum flow rate, V the applied valve voltage, and $V_{1/2}$ the voltage as which half the maximum flow is achieved. Hysteresis was calculated from the difference in $V_{1/2}$ between the opening and closing curves, thus providing a maximum value for the entire curve. The reported maximum flow was estimated from the fit parameter, Q_{max}. However, estimation of the opening and closing voltage are not direct outputs from the Hill equation, thus threshold limits were selected, with respect to Q_{min} for consistent estimates to be made.

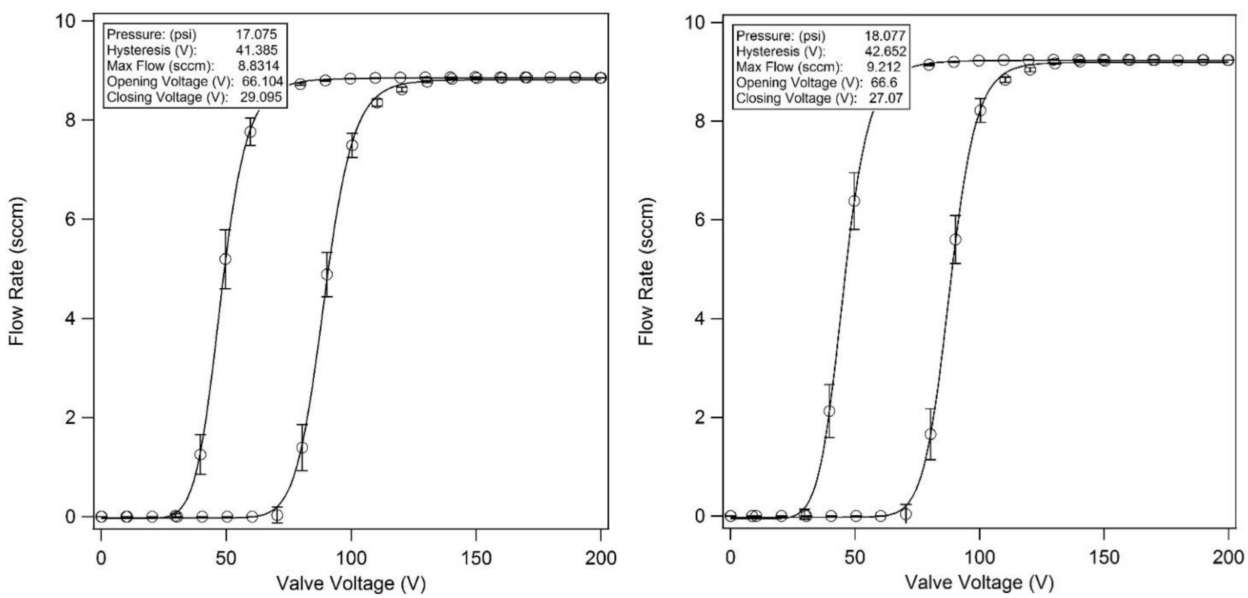

Figure 15. Pre-vibe (left) and post-vibe (right) nitrogen flow curves indicate no appreciable change in performance.

Shifts in opening and/or closing voltage can be indicative of mechanical shifts within the assemble that require micron-level positional repeatability. As can be seen in Figure 15, no shift was observed in the opening or closing voltage of the valve, indicating that sub-micron position accuracy was held through vibration testing. Additionally, flow curve opening and closing hysteresis from the piezo actuator within the assembly remained unchanged, suggesting no actuator damage. The maximum flow observed after vibration testing was slightly higher than that measured before, but was attributed to the difference in supply pressure between the two flow curve captures (pre-vibe: 17psi, post-vibe: 18psi)

2. Thermal Testing

Environmental testing of the 4th generation microvalve followed the same non-operational (0°C to 50°C) and operational (10°C to 30°C) qualification requirements used for LPF. Because the test was performed in ambient pressure, NASA's General Environmental Verification Specification requires ±15°C margin at the extreme ends of both the expected non-operational and operational ranges. Similarly, the minimum of eight operational thermal cycles for component qualification must be increased by 50%, resulting in twelve cycles. Dwell times at the extremes of each cycle may remain at four hours minimum.

The environmental test system consisted of several components that were key to facilitating microvalve immersion in the target environmental conditions. The block diagram in Figure 16 highlights these components. The microvalve, installed onto its test manifold, was enclosed inside a copper box to eliminate the potential for thermal gradients within the valve assembly due to convective losses. More efficient conduction was promoted by using a thermal gap pad as an interface between the test manifold and the copper box. The temperature of the copper box was regulated by a recirculating bath and cold plate, where the cold plate was placed outside the copper box and directly underneath where the microvalve was positioned. A thermocouple installed inside the copper box on the surface shared by the microvalve was used to track actual environmental conditions, as well as a feedback for an automated LabVIEW program. The entire system, other than the recirculating bath, was placed inside an insulating box to further protect against convection and radiation heat loss.

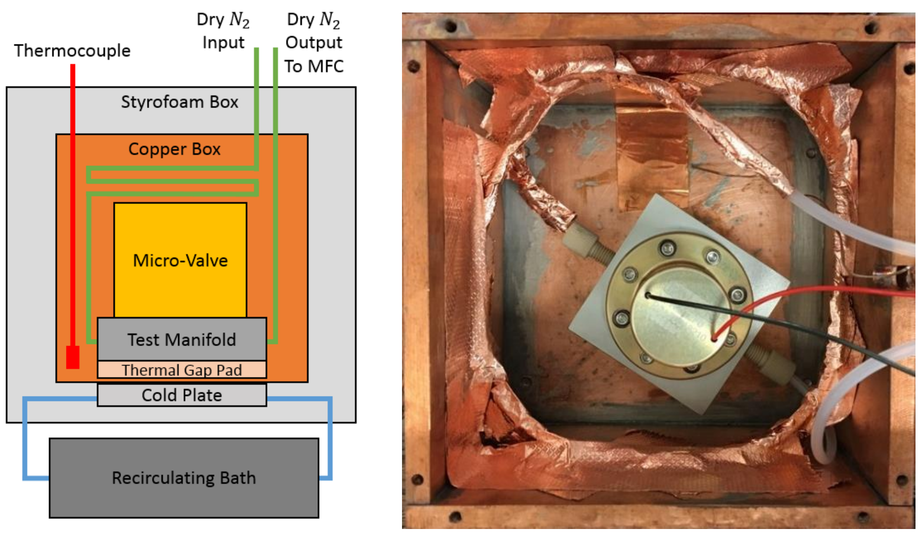

Figure 16. Environmental test system diagram (left). Microvalve inside isothermal copper box.

First order approximations using Eq.(5) and Eq.(6) show that the input tube for nitrogen must be coiled within the copper box a minimum of 3 inches to ensure gas entering the microvalve was at the same temperature as the microvalve body itself. Where Eq (5) was used to calculate the total energy required to bring the nitrogen to temperature, and Eq (6) was used to calculate the conductive heat transfer rate through the tube and into the gas. Combining these equations yielded an expression for time required to reach the target temperature. Minimum tube length was then calculated using this time value and 10sccm maximum flow rate; observed when the valve is wide open and at 17psi tank pressure.

$$Q = mc\Delta T \tag{6}$$

Until formal specifications for the LISA propellant tank are defined, all microvalve tests performed will use the LPF test specification of 17psi. To provide more fidelity to the approximation, the tube was attached to the walls using copper tape then its length was increased to 18inches to further ensure the nitrogen reached the target temperature prior to entering the microvalve (Figure 16, right).

$$Q_c = \frac{2\pi Lk\Delta T}{\ln\left(\frac{r_o}{r_i}\right)} \tag{6}$$

A representative segment of the microvalve's environmental test profile is shown in Figure 17. The profile begins with a functional test to characterize its performance before the thermal cycles. This was immediately followed by a ramp to the hot non-operational temperature of 65°C and soak for 4 hours. The temperature was then brought back down to 23°C for another functional test to verify the microvalve was able to survive this temperature extreme, with no degradation in performance. Similarly, the system was brought down to the cold non-operational temperature of -15°C, soaked for 4 hours, then tested for functionality after being brought back up to 23°C. Hot and cold operational temperature extremes of 45°C and -5°C, respectively, were tested in a similar manner, but included a functional test at each extreme to verify microvalve performance at these temperatures. These operational temperature cycles were then repeated eleven additional times.

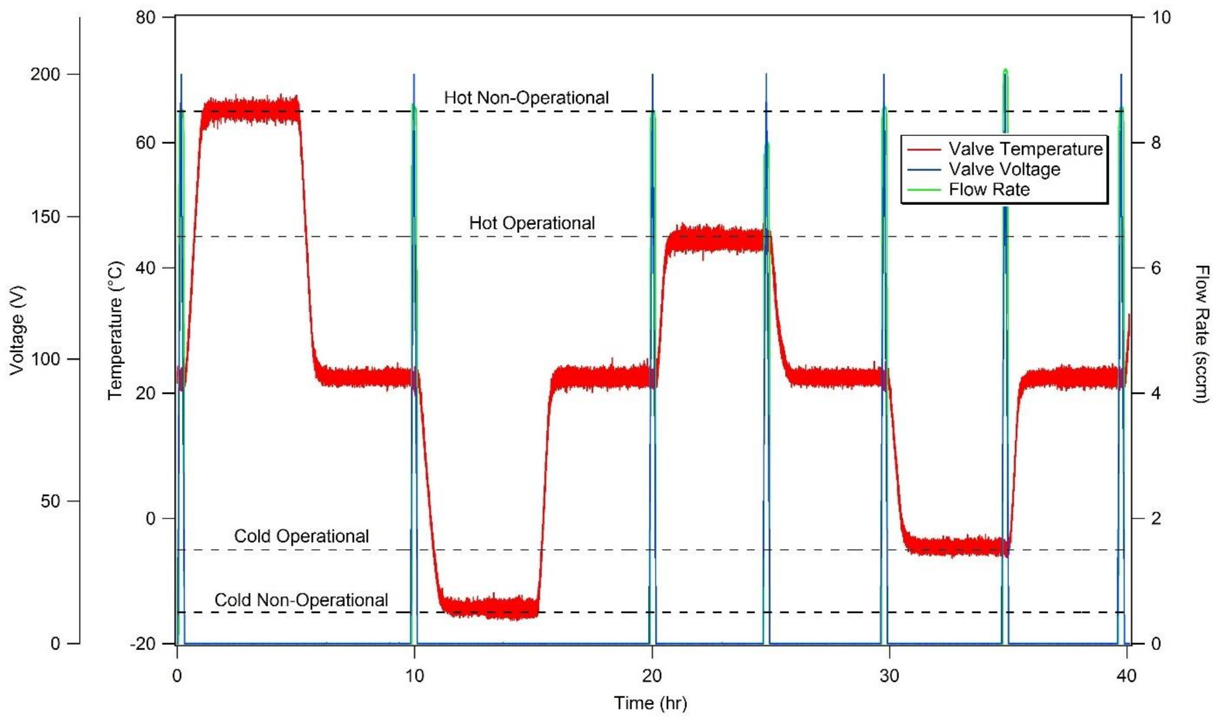

Figure 17. Environmental test profile for 4th Generation Microvalve.

The environmental test profile in Figure 17 along with flow curves generated from each functional test show that this generation microvalve is able to demonstrate survivability across the entire range of non-operational temperatures and functionality across the entire range of operational temperatures. The microvalve remained sealed during the ramp and subsequent soak at the hot and cold non-operational temperature extremes, thus showing it is thermally balanced and able to protect the system from inadvertent propellant flow during these conditions. The graph shown in Figure 18 detail the flow curves and Table 6 lists key microvalve performance parameters at critical nodes of the test profile. The opening and closing voltage were particularly important to monitor during this test. Limited shifts to these values are tolerable and expected. Actuation margin above and below the flow curve are contingencies for such behavior, with maximum allowable deviations identified through the prior flight effort. Ideally, the mid-point of the opening and closing voltage would be set to the middle of the full operating voltage range; however, Figure 18 clearly indicates that this particular microvalve was set to a value below the actuation midpoint. This will be addressed in future microvalve builds. The small variation in these opening and closing voltages throughout the test is further evidence that the microvalve is thermally balanced and thus resilient to performance shifts due to temperature fluctuations. The 10V difference between the opening voltage of the post hot non-operational flow curve and the remaining plots is not yet fully explained and requires additional investigation; however, the subsequent post-cold survival flow curve shows performance in line with the initial functional test, indicating no significant change in microvalve operation. The difference in the maximum flowrate for -15°C, 23°C, and 45°C are the result of flowing gas density changes.

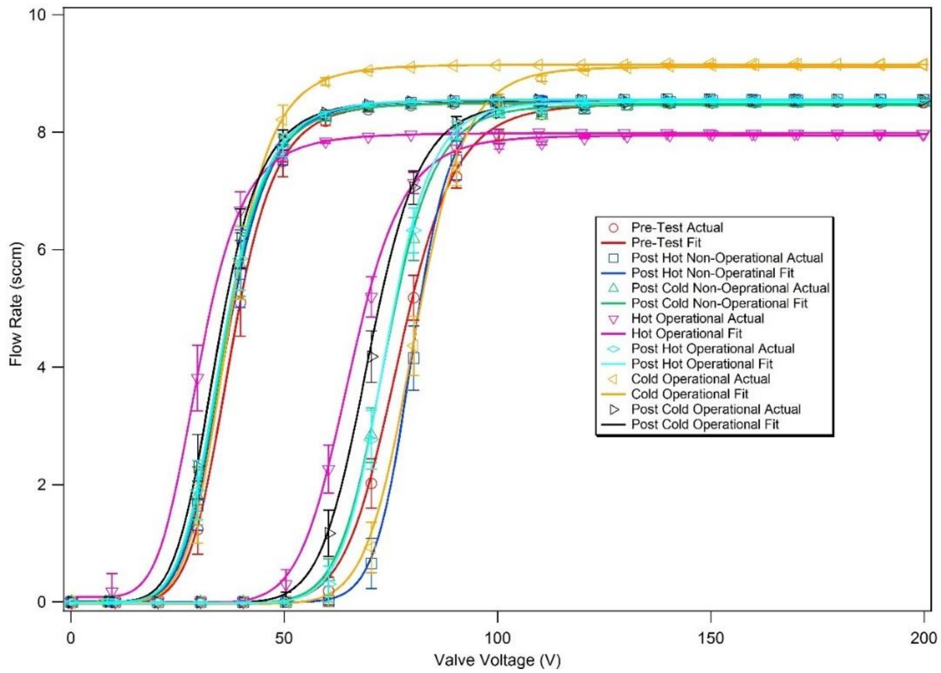

Figure 18. Microvalve flow curves from prior to the test, post hot non-op, and post cold non-op temperature soak.

Table 6. Compiled flow curve parameters verifying nominal valve performance.

Thermal Test Phase	Input Pressure (psi)	Maximum Flow (sccm)	Hysteresis (V)	Opening Voltage (V)	Closing Voltage (V)
Pre-Survival Test	16.2	8.49	39.9	52.7	20.1
Post-Hot Survival	16.7	8.54	44.3	62.6	19.0
Post-Cold Survival	16.4	8.48	38.5	52.4	18.5
Hot Operational	16.4	7.96	35.8	43.0	13.9
Post-Hot Operational	16.4	8.53	38.8	53.5	18.3
Cold Operational	16.2	9.13	44.2	58.4	19.8
Post-Cold Operational	16.4	8.53	36.1	48.1	17.4

B. Accumulator

During thruster non-operation, the two series micro-valves trap propellant within a constrained volume, which may expand due to temperature fluctuations. In a rigid system, the pressure rise from propellant expansion would be sufficient to lift the micro-valve seal and induce unwanted flow. One of two new components in the propellant management system, the accumulator (Figure 19) was designed to act as a compliance for this propellant expansion and contraction. This component was developed in conjunction with the previous generation micro-valve through a NASA SAT program and further redesigned as part of the present effort to eliminate elastomer seals and reduce its overall size. Mechanically simple, the accumulator is an assembly of a base that interfaces with the propellant feed system manifold and a diaphragm that would deflect under pressure. To date, component validation consisted of two tests: volume displacement and permanent deformation measurements.

Figure 19. Accumulator.

1. *Volumetric Displacement*

Validation of Accumulator volumetric displacement was recently reported[11] as part of completed functional testing, with results being shown in Figure. 20 for completeness of the present feed system design discussion. As is apparent, the displacement of the diaphragm within the Accumulator functioned as intended to within the margin placed on the design. The design is tailored for worst-case thermal conditions for the trapped volume between the two microvalves; however, assumes a specific dead volume. Should the dead volume in the final CMTS design be larger than the assumptions made in this design, an updated Accumulator will be necessary.

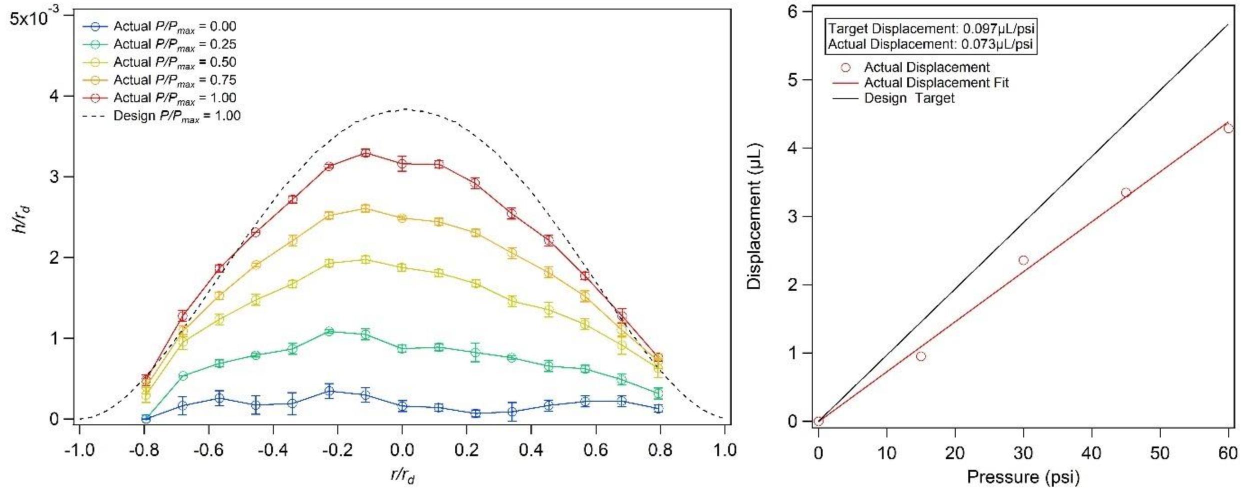

Figure. 20 Distribution of accumulator deformation as a function of pressure (left) and actual vs. target accumulator volume displaced at each pressure (right), indicating the desired linear spring performance. Taken from ref 11.

2. Permanent Deformation

The Accumulator shown in Figure 19 was also tested to pressures up to nearly 5X anticipated tank pressures, as part of a burst test. The Accumulator was pressurized, the was pressure removed and the diaphragm assessed for permanent deformation. The pressure was increased in 50psi increments up to 400psi before being discontinued prior to breaching of the diaphragm. Testing results indicated that permanent deformation did not begin to manifest until beyond 100psi, well above expected thruster operating pressures. Additionally, above this point, deformation was proportional to the applied pressure and was displaced by only a few thousandths of an inch. This suggests that the Accumulator would still function after being subjected to pressures well above worst-case scenarios, but would operate at an altered volumetric displacement rate with respect to feed system pressure.

C. Volume Compensator

The volume compensator is a new propellant flow management system component. Its function was originally serviced by the ST7 micro-valve design, where the downstream volume between the valve and thruster increased upon microvalve closure. This feature pulled propellant back and away from the emitter tips, which provided rapid shutdown and prevented propellant from being expelled due to propellant thermal expansion when non-operational. Similar to the accumulator, the volume compensator addresses the concern over propellant expansion due to temperature fluctuations. In this case, the propellant thermal expansion must overcome the void left by the volume compensator in order to reach the emitter tip.

Originally designed with the accumulator and previous generation micro-valve through the aforementioned NASA SAT program, the volume compensator (Figure. 21) has been further developed to better service the LISA mission. This new generation volume compensator's mechanical design now shares the same inlet base and a similar diaphragm to the accumulator. However, since the volume compensator is to be actively controlled, its diaphragm is mechanically connected to a potted piezo-actuator assembly.

Figure. 21 Volume Compensator.

The worst-case scenario for the volume compensator shares that of the accumulator, wherein the thruster shuts down at the minimum operation temperature of 10°C, trapping propellant between a sealed micro-valve and an open emitter tip, followed by a temperature increase to maximum nonoperation temperature of 50°C. This 40°C temperature rise within that volume was used as a required minimum volumetric expansion for the design; however, a 35% margin was added to the μL-level displacement.

1. Total Volume Displacement

Validation of Volume Compensator displacement was recently reported[12] as part of completed functional testing, with results being shown in Figure 22 for completeness of the present feed system design discussion. The Volume Compensator was filled with liquid, with its output connected to a capillary that terminated on a mass balance. Volumetric actuation of the Volume Compensator was measured by recording the mass change on the balance. The design point for the present Volume compensator is on the order of a few microliters; however, the finalized design is dependent on the dead volume in updated system-level configuration. To verify its maximum volume displacement capacity, the volume compensator's piezo-actuator was charged to its maximum voltage (V_p/V_{pmax}=1). A set of five displacement measurements (dV) were acquired to obtain an averaged displacement, with the results normalized to the designed displacement (dV_d). As can be seen, the actual measure displacement (red dashed line) was approximately 93% of the original design (black dashed line).[11]

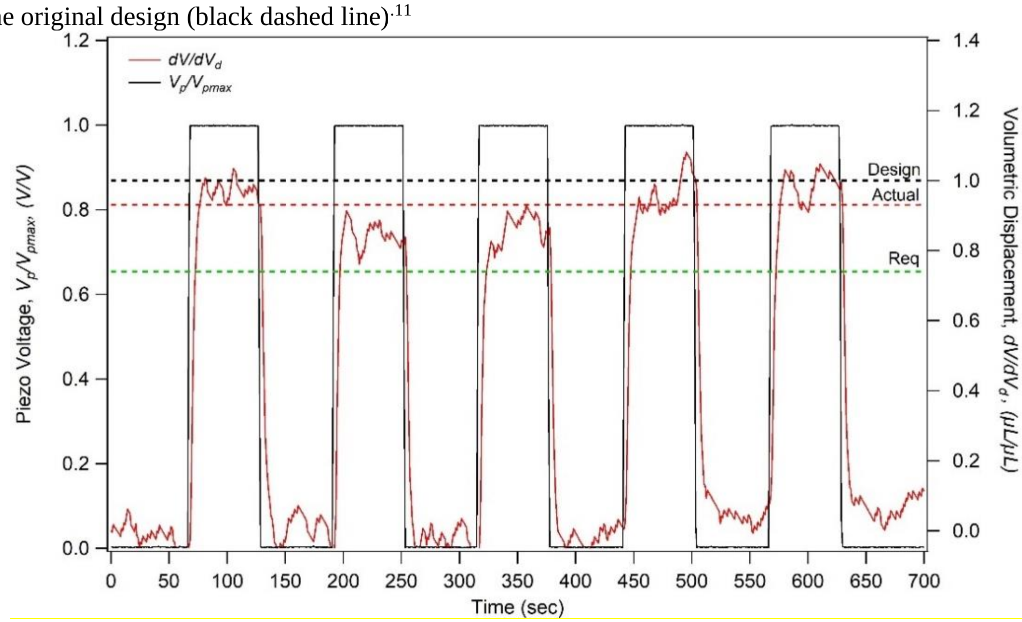

Figure 22. Volume displacement validation test results. Taken from ref 14.

Additional thermal testing is anticipated in the coming months, to verify proper Volume Compensator function over both survival and operational temperature ranges. The true position of the elements within the volume compensator are not critical, as they are within the microvalve, the differential displacement generated by the actuating piezo within is the primary design parameter. However, that movement that generates the volumetric displacement is still on the order of microns, meaning that thermal expansion or contraction of the mechanical elements can impact the volumetric displacement. Materials selections within the Volume Compensator were selected to have a neutral to slightly beneficial effect with respect to temperature, but this still remains to be validated.

2. Proportional Volume Displacement

The Volume Compensator is not intended to be a dynamic element during thruster operation, essentially operating either fully energized when operational or deenergized when disabled. However, it should be noted that the Volume Compensator holds sufficient propellant to support several minutes of operation at LPF nominal thrust conditions (20μN). Proportional volumetric control has been demonstrated in case it is determined to be necessary during thruster startup or shutdown conditions where, if actuated near instantaneously, a thruster flooding condition could result. Instead propellant could be gradually emitted via electrospray at an appropriate flow rate. The Volume compensator was actuated from 0V to 200V in 10V increments, with the displaced volume recorded at each and returning to 0V between each step. The results of this displacement test indicated a relatively linear volumetric response with respect to the applied piezo voltage.[11]

D. Thruster Head

The thruster head manifold (Figure 23) distributes the propellant flow from the upstream FCA to each of the nine emitters on the thruster head. Busek utilizes various bubble elimination mechanisms to aid with water bubble rejection during startup; as previously state, residual water elimination is only an issue during initial thruster commissioning.

Busek has patented the method of using gas permeable membranes to aid in bubble rejection from the feed system. The original LPF design utilized a tubular bubble eliminator. The present manifold transitioned to a planar-style bubble eliminator that simplified the design, eliminated multiple seals, and reduced dead volume within the manifold. Tests were developed to validate proper sealing of the new manifold design, as well verify the permeability and structural integrity of the gas permeable membrane.

3. Leak Testing

A key concern with regards to changes in the thruster manifold are leaks, particularly with respect to sealing of the gas permeable membrane, thus leak testing was performed to validate the design. To assess for leaks, the manifold was pressurized to nominal operating pressures via the propellant inlet while monitored by a pressure transducer for a potential loss of pressure once isolated. Once the pressure was set, the manifold was isolated and the pressure logged over the course of hours. This test was performed six times on one assembly that had been dis-assembled and re-assembled multiple times, with no discernable pressure decay evident. There were no observed changes in the pressure within the thruster manifold after being isolated, suggesting that there were no measurable leaks in the assembly tested.

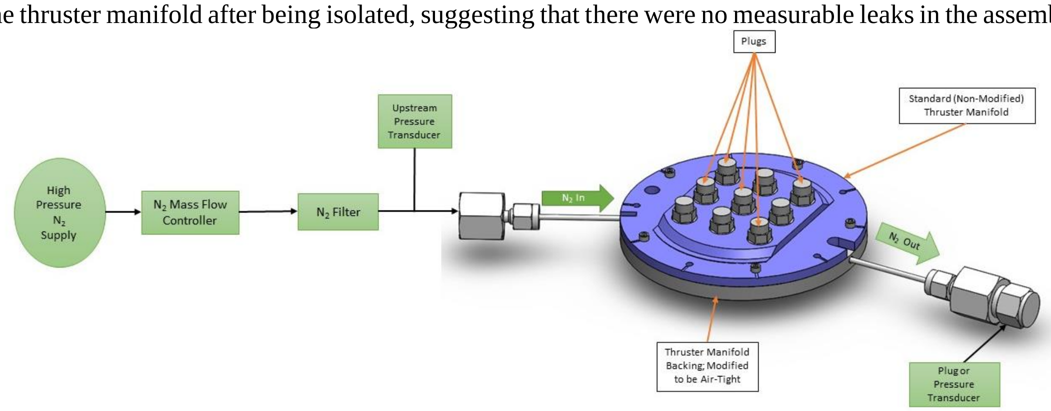

Figure 23. Thruster head manifold leak test setup.

4. Vibration Testing

Vibration testing was performed on the manifold per NASA General Environmental Verification Standards (GEVS) for component-level workmanship (Table 7). The manifold was vibration tested in all three axes (Figure 24), with low level sinusoidal sweeps performed before and after a 60 second random vibration to assess for changes in response that could potentially indicate damage. A control accelerometer mounted to the vibration test fixture was used for closed loop control of the vibration table to the desired levels, while a second accelerometer mounted to the top of the manifold was used for measuring the response of the device under test.

Table 7. Table 6. GEVS component minimum workmanship random vibration test levels for 45.4kg (100lbs) or less.

Frequency (Hz)	ASD Level (g^2/Hz)
20	0.01
20-80	+3 dB/oct
80-500	0.04
500-2000	-3 dB/oct
2000	0.01
Overall	6.8 g_{rms}

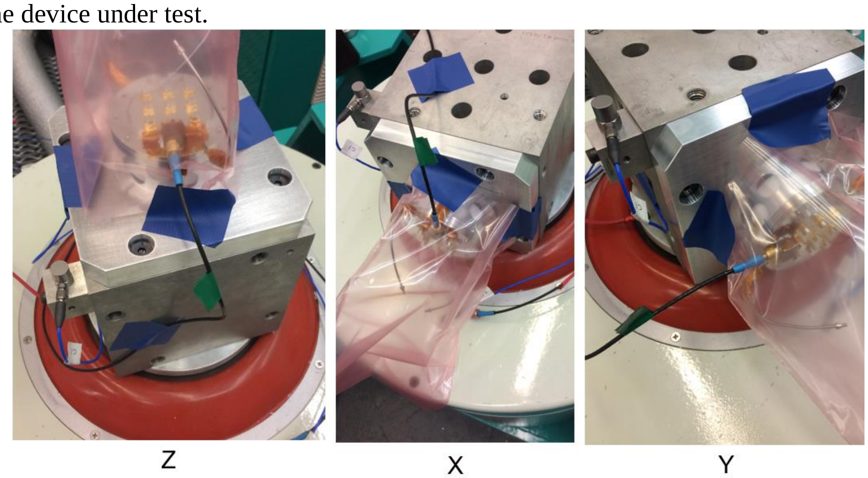

Figure 24. Thruster Head Manifold undergoing vibration testing in three axes.

Before and after vibration testing, the manifold is subject to a nitrogen pressure test to assess for any leaks in the assembly or changes in the characteristics of the gas-permeable membrane caused by vibration. The pre-vibe pressure and permeation tests shown indicated that the manifold was leak free and ready for random vibration testing. As stated above, the manifold was tested in all three axes per GEVS standards for component level workmanship. Figure 25 through Figure 27 show a sample of the x-axis test, with sine sweeps included before and after random vibe included. For all test cases, no significant vibrational response shifts were detected within the assembly by the accelerometers, indicating that no discernable damage took place within the assembly. This conclusion is supported by the post-vibe pressure and flow tests recorded, which were identical to those obtained before the vibration tests. There is a significant response above the input vibration level at high frequencies and is due to the propellant feed line to the thruster manifold that was not connected and only partially supported during testing. Again, and as noted with microvalve vibration testing, a peak at approximately 180Hz is test setup related.

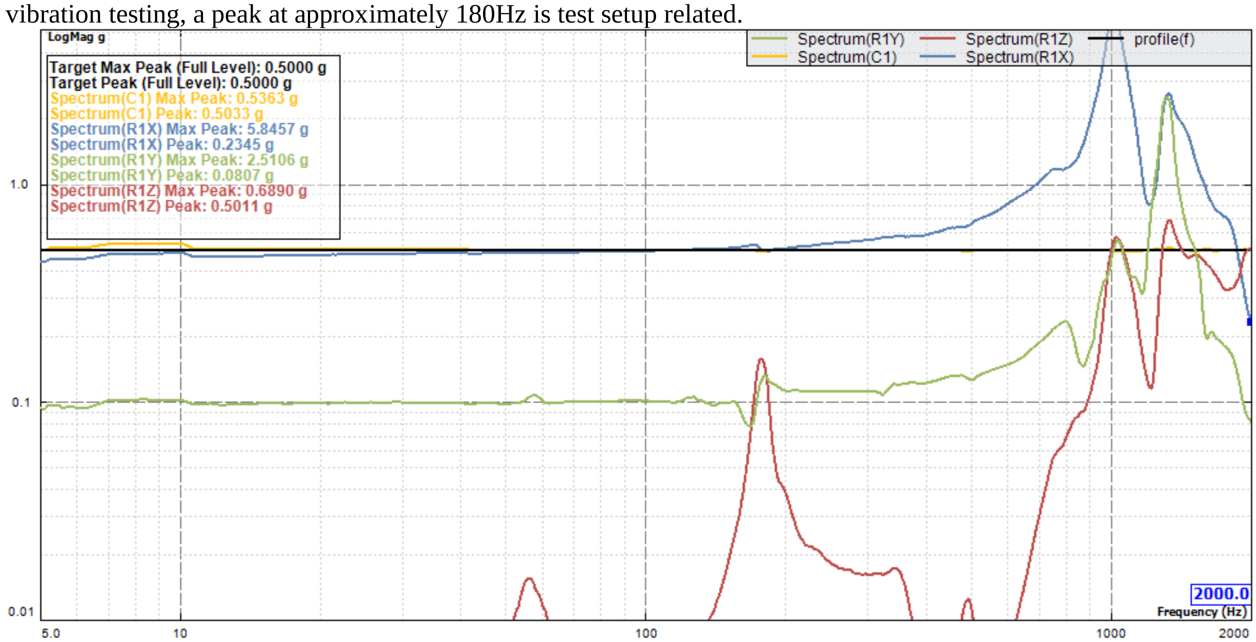

Figure 25. Manifold low-level sine baseline sweep, x-axis.

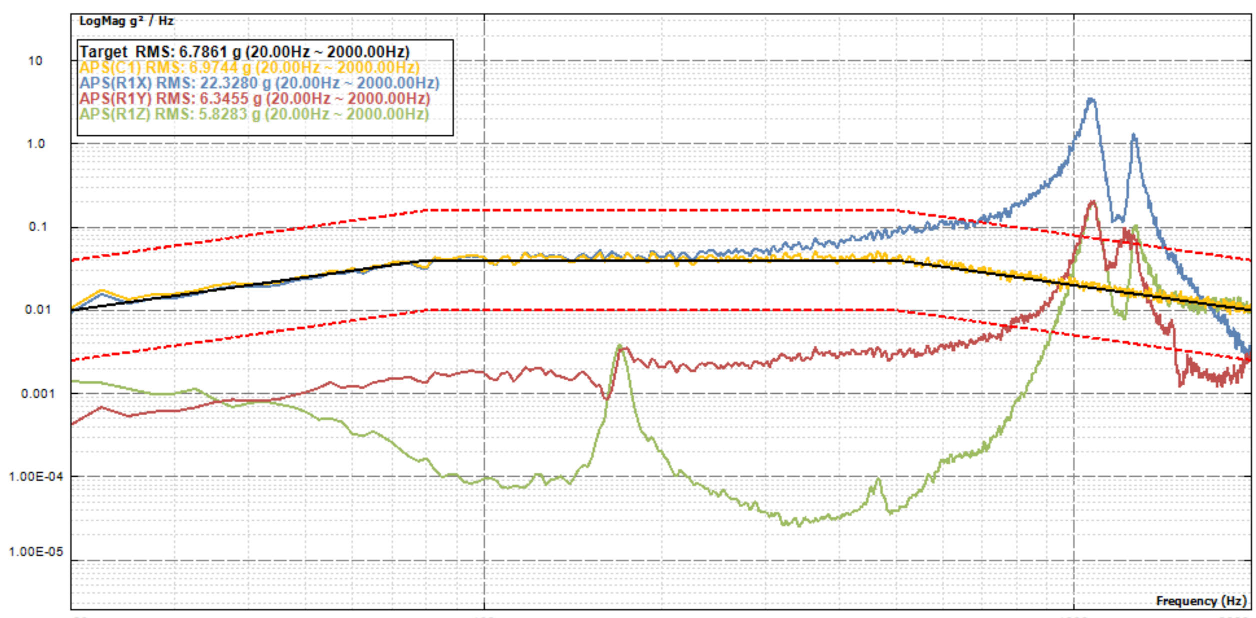

Figure 26. Manifold x-axis random vibration test.

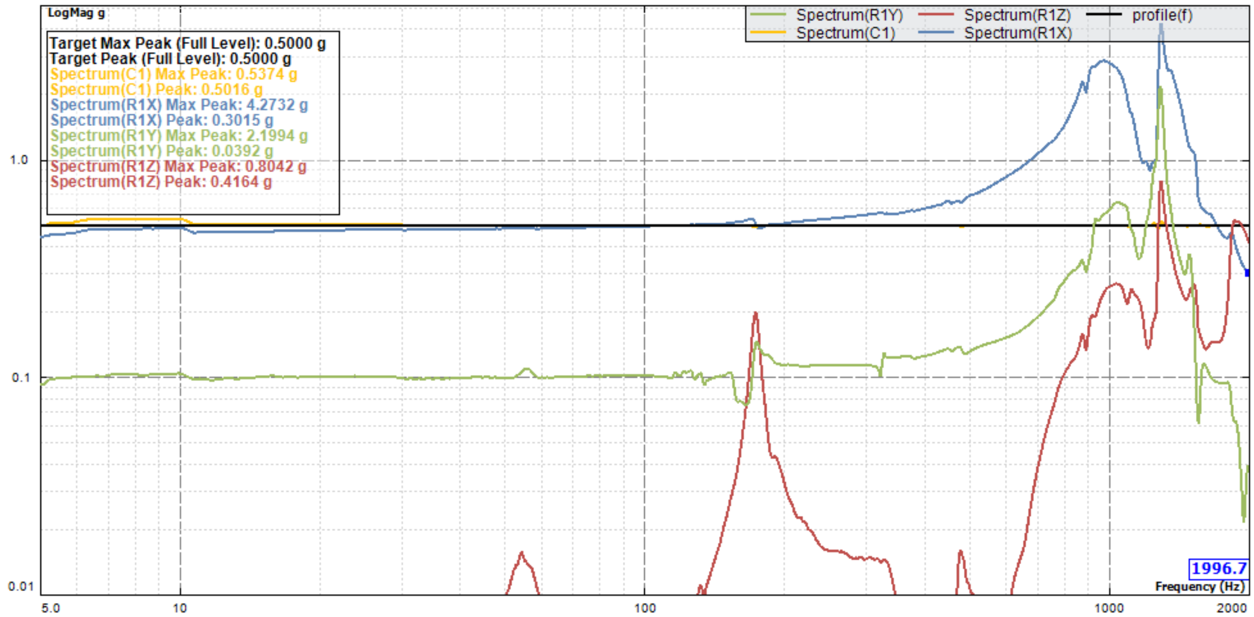

Figure 27. Manifold low-level sine post-vibe sweep, x-axis.

E. Capillary Emitters

1. Capillary Emitter Design

The basic functional design of the flight-qualified capillary emitters developed for LPF remain unchanged, with a flight emitter shown in the left image of Figure 28 and a partially completed emitter from the present emitter build shown on the right. The three key elements of the emitter remain to be: 1.) a brazed base to allow for fluidic connection to the thruster manifold, 2.) a stem for wrapping of the capillary length in a compact space, and 3.) a height adjustable emitter tip used for achieving the desired emitter-to-extractor spacing.[11] The design changes implemented to date impact fabrication, not the functionality of the end assembly. Due to the large quantities of emitters that would be needed as part of a LISA mission flight build, changes focused on eliminating high risk or labor intensive fabrication steps that could result in reduced production yield and protracted production schedules.


Figure 28. Capillary emitter fabricated for LPF (left) and emitters recently fabricated (right) to support future testing.

2. Flow Impedance Matching Criteria

All capillary emitters are flow impedance tested after each step in the fabrication process as a validation that the capillary is intact and remains suitable for use. Combined batch acceptance criteria are then applied to the collected flow impedance data before moving forward to the next fabrication step or final thruster head grouping. The left graphic of Figure 29 shows a standard deviation histogram of both the LPF flight capillaries tubes (109 emitters) and most recent builds (41 capillaries), prior to fabrication into final emitter assemblies. Capillaries with anomalous flow impedances are screened out and tend to skew towards higher impedances with respect to the mean and are potentially due to mechanical or particulate damage during the fabrication process. After anomalous emitters have been discarded, emitters within one standard deviation are sorted and matched into groups that minimize variations in flow impedance within the final assembled thruster. The actual impedance can vary considerably from the theoretical calculated from

Eq.(1). Flow impedance of these capillaries is highly dependent on the accuracy of the inner diameter, as $Z \propto r^4$. As a result, inner diameters only a few microns can readily explain the difference (LPF Build: +6.5µm & Recent Build: -2.7µm).[11] For this reason, emitters fabricated from different batches of stock capillary tubing are not mixed.

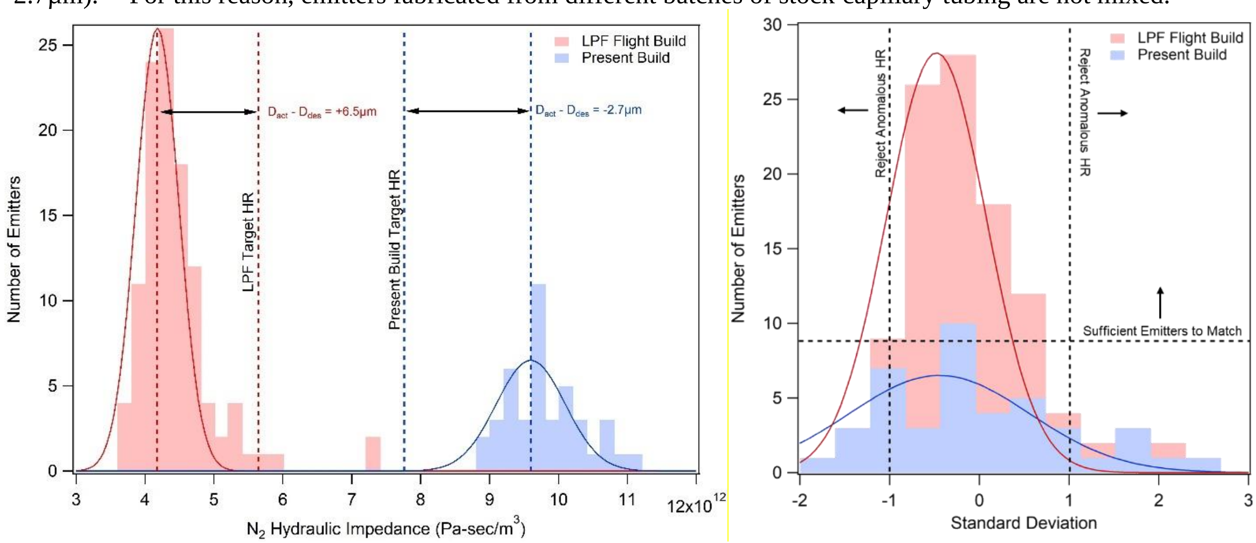

Figure 29. Targeted and measured average hydraulic impedance (left) and batch hydraulic impedance distribution, with acceptance criteria (right), for LPF and recent capillary emitter builds. Taken from ref 11.

3. Emitter Assembly Fabrication Results

Once raw emitters have been processed and flow impedance tested, outliers are discarded and the remaining capillary tubes are processed into emitter assemblies, as shown in Figure 28. The discarding of outliers typically narrows the distribution, which is seen in the LPF flight build data shown in Figure 30. The standard deviation of the distribution was reduced from 4.39×10^{11} Pa-sec/m^3 to 3.31×10^{11} Pa-sec/m^3. Additionally, the average flow impedance dropped by 8% from the processed capillary to final emitter assembly. This can be attributed two process features: 1.) outlier hydraulic impedances are typically higher than the mean and are a result of a defect that interrupts flow, thus are more likely to be discarded, and 2.) some excess capillary length is trimmed as part of the final fabrication step, but this is weakly related to impedance, as compared to tube inner diameter ($Z \propto L$ vs $Z \propto r^4$).

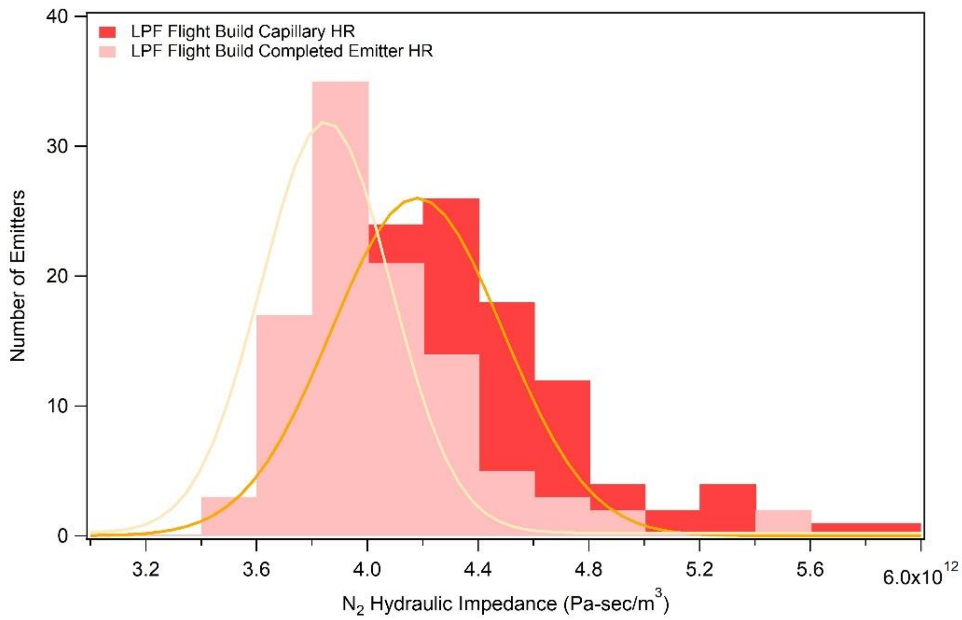

Figure 30. Processed capillary tube versus final processed emitter assembly hydraulic impedance.

The flow impedance of the processed capillaries and finished emitter assemblies from the most recent production batch are shown in Figure 31. There is less of a shift in the absolute flow impedance between raw capillary and final emitter assembly, as compared to the previous flight build. This can be attributed to improved handling and procedures, as well as reduced post-braze trimming requirements, again through improved procedures. There are sufficient completed capillary emitter assemblies to produce two 9X capillary emitter thruster heads that meet previously determined flow matching requirements, focusing on emitters between 9.5x10^{12} Pa-sec/m^3 and 10.5x10^{12} Pa-sec/m^3. Future work will include integrating these emitters into a thruster head to support future integrated testing.

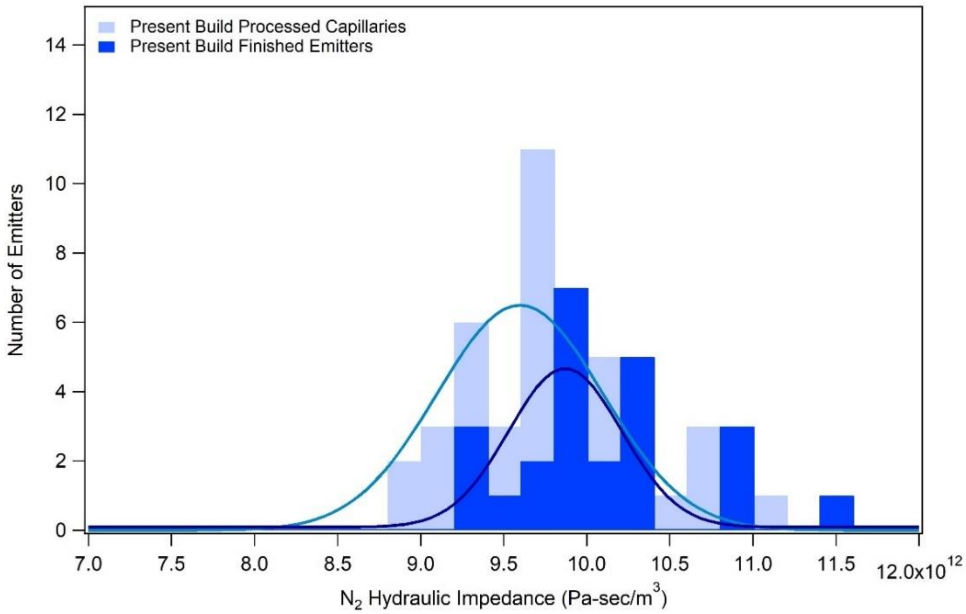

Figure 31. Processed capillary tube versus final processed emitter assembly hydraulic impedance.

V.Conclusion

Busek has initiated continued development of the CMTS system towards meeting the requirements for the European Space Agency LISA mission. Lessons learned from flight hardware development, on-orbit operations, and additional investigations have been compiled, prioritized, and used as justification for updates to the prior flight design. Updated Thruster String Assembly components have been designed and fabricated, and initial functional testing is complete. The 4th generation Busek microvalve has successfully passed through functional, vibrational, and is not in thermal testing. Through this environmental testing, the valve has demonstrated performance equivalent or better than the flight heritage design flown as part of the LPF mission. Additionally, fabrication processes have been improved and have resulted in high production yield from base parts to final tested assembly. Updated assembly fixturing has been designed and fabricated to support the mass production that would be necessary as part of a potential LISA mission flight opportunity. New feed system elements, such as the Accumulator and Volume Compensator have been demonstrated to function as intended.

Preliminary LISA spacecraft designs produced by the ESTEC Concurrent Design Facility are considerably larger than LPF, suggesting increased thrust levels may be necessary. In order to be responsive to ongoing mission studies, Busek has developed CMTS mass estimates as a function of thrust capability. Busek believes that the colloid propulsion system discussed herein presents a significant mass savings opportunity to the LISA spacecraft, as compared to the present ESA cold gas baseline design. These mass savings are largely driven by propellant mass savings afforded to the colloid system due to the increased specific impulse (150-250sec), as compared to cold gas (45-60sec). To further support the potentiality of increased thrust requirements, Busek has performed a propellant feed system analysis to assess its ability to support increased thrust levels. Due to the increased propellant pressurization anticipated in the CMTS design for LISA (2.5atm @ EOL for LISA, vs 1atm for LPF), similar or greater feed system flow capability margins are maintained up to thrusts 4X greater than that demonstrated on LPF. This suggests that the present feed system elements likely require no modifications to support required maximum thrust levels up to ~150μN.

Capillary emitter fabrication has been updated to eliminate high risk and labor-intensive steps in order to support the mass production that may be necessary for a LISA propulsion system flight build. This has been accomplished without changing the basic function or critical geometries necessary to retain the well-characterized performance of the prior flight thruster. Criteria for acceptance/rejection of emitters at each step of the fabrication process have been improved and incorporated onto updated procedures.

Component-level environmental testing is presently nearing completion and will be followed by additional productions runs and integration of these components into their major subassembly groups (e.g. FCA, PMA, & Thruster). Repeated environmental testing at the subassembly level shall be followed by assembly of a complete Thruster String Assembly in preparation for initiating both performance and life testing. Should Busek's CMTS technology be selected by NASA and ESA as a contribution to the mission, this timeline is compatible with the present ESA anticipated launch date.

Acknowledgments

This research was performed by Busek under a subcontract with the Jet Propulsion Laboratory, California Institute of Technology, with support from the National Aeronautics and Space Administration (NASA) via the LISA Study Office and Physics of the Cosmos (PCOS) program.

References

.

[1] J. Zwahlen, et al., "Flow Control Micro-valve for the ST7-DRS Colloid Thruster", 44th Joint Propulsion Conference, Hartford, CT, AIAA-2008-4930, July 2008.

[2] T. Roy, et al., "Direct Thrust Measurements of ST7 Colloid Micro-Newton Thruster", 44th Joint Propulsion Conference, Hartford, CT, July 2008.

[3] N. Demmons et al., "ST7-DRS Mission Colloid Thruster Development", 44th Joint Propulsion Conference, Hartford, CT, AIAA-2008-4823, July, 2008.

[4] V. Hruby, et al, "ST7-DRS Colloid Thruster System Development and Performance Summary", 44th Joint Propulsion Conference, Hartford, CT, AIAA-2008-4824, July, 2008.

[5] D. Spence, et al., "Colloid Thruster Propellant Conditioning and Storage for the NASA ST7 Mission", 44th Joint Propulsion Conference, Hartford, CT, July 2008.

[6] E. Ehrbar, et al., "Power Processor for the Colloid Micro-Newton Thrusters for the JPL DRS/ST7 Mission", 44th Joint Propulsion Conference, Hartford, CT, July 2008.

[7] N. Demmons et al., "Electrospray Thruster Propellant Feedsystem for a Gravity Wave Observatory Mission", 52nd AIAA/SAE/ASEE Joint Propulsion Conference, AIAA Propulsion and Energy Forum, AIAA 2016-4739, Salt Lake City, UT, 2016.

[8] P. Maghami, J.R. O-Donnell, Jr., O.H. Hsu, J.K. Ziemer, and C.E. Dunn, "Drag-Free Performance of the ST7 Disturbance Reduction System Flight Experiment on the LISA Pathfinder", 10th International ESA Conference on Guidance, Navigation & Control Systems, May 29th to June 2nd, Salzburg, Austria, 2017.

[9] J.K. Ziemer, et. al., "Colloid Microthruster Flight Performance Results from Space Technology 7 Disturbance Reduction System", The 35th International Electric Propulsion Conference, Georgia Institute of Technology, USA, October 8 – 12, 2017.

[10] N. Demmons et. al., "Colloid MicroNewton Thruster (CMNT) System Design Updates Towards Meeting LISA Mission Requirements", The 4S Symposium, May 28th – June 1st, 2018, Sorrento, Italy.

[11] N. Demmons et. al., "Component-Level Development and Testing of a Colloid Micro-Thruster (CMT) System for the LISA Mission", 55th AIAA/SAE/ASEE Joint Propulsion Conference, AIAA Propulsion and Energy Forum, AIAA 2019-3815, Indianapolis, IN, 2019.